

Digitally reconfigurable binary coded terahertz metamaterial with output analogous to NOR and AND

Chong Pei Ho, Prakash Pitchappa, and Chengkuo Lee

Citation: [Journal of Applied Physics](#) **119**, 153104 (2016); doi: 10.1063/1.4946891

View online: <http://dx.doi.org/10.1063/1.4946891>

View Table of Contents: <http://scitation.aip.org/content/aip/journal/jap/119/15?ver=pdfcov>

Published by the [AIP Publishing](#)

Articles you may be interested in

[Terahertz response of fractal meta-atoms based on concentric rectangular square resonators](#)

J. Appl. Phys. **118**, 193103 (2015); 10.1063/1.4936217

[Ultra-high Q even eigenmode resonance in terahertz metamaterials](#)

Appl. Phys. Lett. **106**, 011102 (2015); 10.1063/1.4905478

[Ultrabroadband reflective polarization convertor for terahertz waves](#)

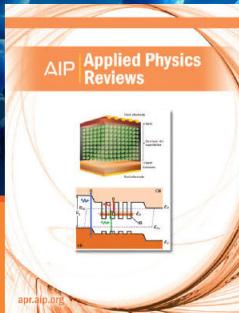
Appl. Phys. Lett. **105**, 181111 (2014); 10.1063/1.4901272

[Reconfigurable liquid metal based terahertz metamaterials via selective erasure and refilling to the unit cell level](#)

Appl. Phys. Lett. **103**, 221116 (2013); 10.1063/1.4837675

[Polarization-sensitive microelectromechanical systems based tunable terahertz metamaterials using three dimensional electric split-ring resonator arrays](#)

Appl. Phys. Lett. **102**, 161912 (2013); 10.1063/1.4803048



NEW Special Topic Sections

NOW ONLINE
Lithium Niobate Properties and Applications:
Reviews of Emerging Trends

AIP | Applied Physics Reviews

Digitally reconfigurable binary coded terahertz metamaterial with output analogous to NOR and AND

Chong Pei Ho, Prakash Pitchappa, and Chengkuo Lee^{a)}

National University of Singapore, 4 Engineering Drive 3, Singapore; Center for Intelligent Sensors and MEMS, National University of Singapore, 4 Engineering Drive 3, Singapore 117576, Singapore; and NUS Suzhou Research Institute (NUSRI), Suzhou Industrial Park, Suzhou 215123, People's Republic of China

(Received 3 February 2016; accepted 4 April 2016; published online 19 April 2016)

We experimentally demonstrate a digitally reconfigurable binary coded terahertz metamaterial in the Terahertz (THz) frequency with the transmission output analogous to NOR and AND logic. An electric split-ring resonator with a released central arms is used as the switchable meta-bit. Isolation of controls in adjacent meta-bits allows for three distinct reconfiguration states of the metamaterial with the output analogous to **NOR** and **AND** at 0.26 THz and 0.36 THz, respectively. Further enhancement in controllability at the unit cell level will aid in the development of dynamically programmable metamaterial operating in the transmission mode for THz frequencies. *Published by AIP Publishing.*
[\[http://dx.doi.org/10.1063/1.4946891\]](http://dx.doi.org/10.1063/1.4946891)

I. INTRODUCTION

Research in the terahertz (THz) region of the electromagnetic (EM) spectrum has gained speed due to its potential to be used in many applications such as next generation high speed wireless communication systems.^{1,2} At present, the ability to control and manipulate THz waves, such as active filters to display logic functionalities, is highly sought after for the realization of sophisticated THz communication systems. One problem with THz waves is that they have minimal interaction with the naturally occurring materials.^{3,4} In order to overcome this limitation, an array of subwavelength structures termed as metamaterials are explored to achieve desired THz properties. Metamaterial properties are primarily dependent on the pattern size and shape and have led to the demonstration of various interesting properties in the THz region.^{5,6} Furthermore, active tuning of THz properties is also reported through various methods such as the inclusion of a semiconductor diode to change the capacitance of the resonators media,^{7,8} the change in the property of surrounding media,⁹ and the control of conductivity of doped semiconductor material into the unit cell design.¹⁰ Tunability in metamaterials provides a new dimension for advanced manipulation of THz waves. However, the use of active materials for achieving tunability is not highly scalable as their material properties are often frequency dependent.

Alternatively, microelectromechanical systems (MEMSs) that are well developed for the realization of three-dimensional movable structures are integrated into the metamaterial unit cell geometry. Through the electrical or thermal stimulus, the MEMS structures are physically deformed to achieve structural reshaping of the metamaterial unit cell. Microactuators integrated into the metamaterial unit cell geometry can achieve either in-plane or out-of-plane reconfiguration.^{11–20} MEMS reconfigurable metamaterials have an unparalleled advantage of being highly miniaturized, electrically controlled, and

readily integrated with ICs and detectors, thus making them the perfect choice for high performance tunable THz devices.

Recently, coding metamaterial has been reported as a new class of metamaterial, whereby the EM properties of the metamaterial can be determined by a coding sequence.^{20–24} The unit cell with reflection phase of 0 and π was considered as “0” and “1” states, and by placing the meta-bits in a particular coding fashion, the microwave reflected beam profile and direction was altered. The coding metamaterial was scaled up to the multi-bit system by designing more number of meta-bits with varying reflection phase and this provides room for finer definition of the reflection profile of incident microwaves. More interestingly, dynamically switchable unit cell was also reported by integrating diodes. By actively switching the meta-bit from OFF to ON state, the reflection phase was changed from 0 to π . This enabled the demonstration of dynamically programmable metamaterial, where the desired reflection profile of the incident microwave was readily achieved through actively programming the coding sequence. Reports of coding metamaterial based on the reflection phase was also reported in the THz spectral region.^{21,23,24} Research has also taken flight in order to realize metamaterials that are able to produce logic-gate operations. Natural memory media such as phase-change materials have been typically used, but they require thermally isolated environment to operate or require a strong optical pump.^{25–27} More recently, Kim *et al.*²⁸ have shown the use of electrical inputs in a reconfigurable logic-gate metadvice realized by hybridization of graphene to achieve two-input logic-gate operations such as **AND**, **OR**, and **XOR** at room temperature.

In this work, we experimentally demonstrate a dynamically switchable binary coding metamaterial, with the state of meta-bit defined by the THz transmission intensity, instead of the reflection phase. The conventional electrical split ring resonator (eSRR) is used as a meta-bit for a proof-of-concept demonstration. The central arms forming the in-plane gap of the eSRR are released with an air gap between the arms and the silicon (Si) substrate. Such pre-stressed cantilevers can be

^{a)}Author to whom correspondence should be addressed. Electronic mail: elelc@nus.edu.sg

seamlessly integrated with the complex metamaterial unit cell geometry and have been shown to be highly sufficient for the display of advanced THz functionalities such as anisotropy switching, active chiral metamaterials, etc.^{13–16,18–20} The position of the released arms can be deformed electrostatically by applying the voltage between the arms and the Si substrate. Based on the physical position of the released arms, the state of the meta-bit is defined. The control lines to adjacent meta-bits are isolated and hence this allows for the metamaterial to be in one of the three unique states. Through this control scheme, the transmission response of the metamaterial produces outputs analogous to NOR and AND in pursuance of achieving digital outputs at room temperature as shown in Fig. 1. Ideally, when the voltage is removed, the suspended arms will restore to their initial position. However, it was observed that the arms across the unit cells pull out at different times due to the non-uniformity in fabrication. Such effects can be reduced to make the actuation of the suspended arms in this device repeatable by introducing dimples.^{29,30}

II. DESIGN, SIMULATION, AND FABRICATION OF DEVICE

The geometrical parameters for the eSRR meta-bit are shown in Fig. 2(a). The periodicity of the metamaterial (P) is $120\ \mu\text{m}$, the width (W) is $4\ \mu\text{m}$, the central arm length (I) is $30\ \mu\text{m}$, the tip length (G) is $20\ \mu\text{m}$, the side length (L) is $80\ \mu\text{m}$, and the split gap is $4\ \mu\text{m}$. Based on these parameters, the capacitive coupling between the eSRRs is negligible as the two eSRR meta-bits are kept far apart.^{31,32} The digital metamaterial is fabricated on an 8-in. Si wafer using the complementary metal-oxide-semiconductor (CMOS) compatible process.¹³ The process starts with the deposition of a $100\ \text{nm}$ thick silicon dioxide (SiO_2) as the sacrificial layer. The SiO_2 layer is patterned and etched to define the anchor and a $20\ \text{nm}$ thick aluminium oxide (Al_2O_3) and a $500\ \text{nm}$ thick aluminium (Al) are deposited. The eSRR patterns are then patterned and etched through the Al/ Al_2O_3 stack. The central arms of eSRR unit cells are released by isotropically dry etching the SiO_2 sacrificial layer using vapour hydrofluoric acid

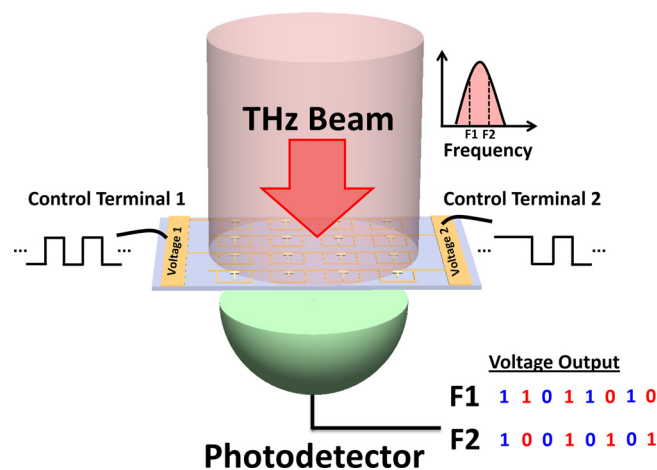


FIG. 1. Schematic of the proposed binary coded digital metamaterial for the control of output intensities at specific frequencies to provide EM analogous to logic outputs. The control scheme is done through the voltage inputs at control terminals 1 and 2.

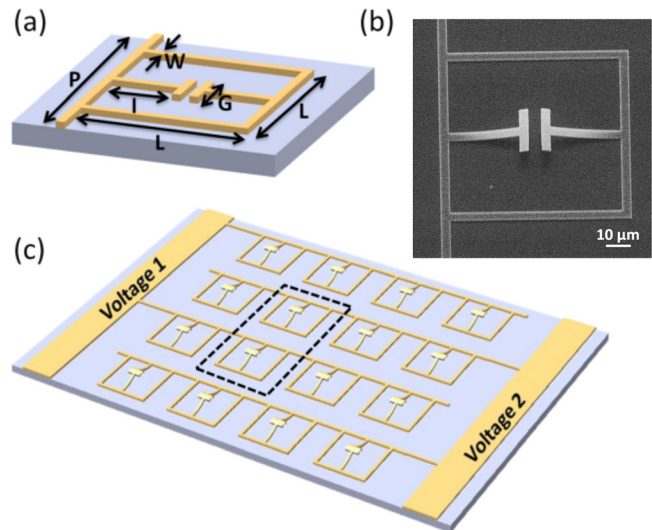


FIG. 2. (a) Schematic drawing of the eSRR meta-bit with geometrical parameter definitions and (b) the fabricated the meta-bit with central arms released. (c) 3D schematic representation of the digital metamaterial with the isolated control of adjacent eSRRs and so the two eSRRs within the unit cell can be switched separately. The dashed line represents the effective unit cell of the metamaterials.

(VHF).^{13–20,33,34} After the release step, the central arms along the split bend up due to the residual stress layers. Hence, the initial air gap between the tip of the released cantilevers and Si substrate is much higher than the sacrificial layer thickness. The measured initial tip displacement of the fabricated eSRR arms is $2\ \mu\text{m}$. The scanning electron microscope image of the fabricated eSRR meta-bit after the release step is shown in Fig. 2(b) and it clearly shows the out of-plane deformed profile of the released arms. The electrical connections between the adjacent meta-bits are isolated and hence can be controlled independently as shown in Fig. 2(c).

When the voltage is applied across the released cantilevers and Si substrate, the attractive electrostatic force pulls the released cantilevers towards the Si substrate. When the applied voltage is higher than the pull-in voltage, the movable cantilevers will come in physical contact with Si substrate. In this work, the pull-in voltage is found to be $30\ \text{V}$. Based on the physical position of the released cantilevers, the state of the meta-bit is defined as OFF state when no voltage is applied and the arms are released and as ON state when the arms are actuated by applying higher voltage to be in physical contact with Si substrate. The adjacent meta-bits can be controlled by biasing terminal 1 and terminal 2, respectively. The voltage at terminal 1 and terminal 2 is referred to as “V1” and “V2,” respectively. By varying the voltage bias at V1 and V2, three unique configuration states of the metamaterial can be realized as depicted in Figs. 3(a)–3(c). The optical microscope images are also shown from Figs. 3(d)–3(f) for the different states illustrated. When both V1 and V2 are at the same potential as the substrate and both the eSRRs in the unit cell have the released cantilevers bend upwards, this configuration will be considered as **State 1**. When a high voltage is applied at either V1 or V2, the released cantilever of only one eSRR is snapped down to the substrate and this configuration is considered to be **State 2**. **State 2** can be realized by switching

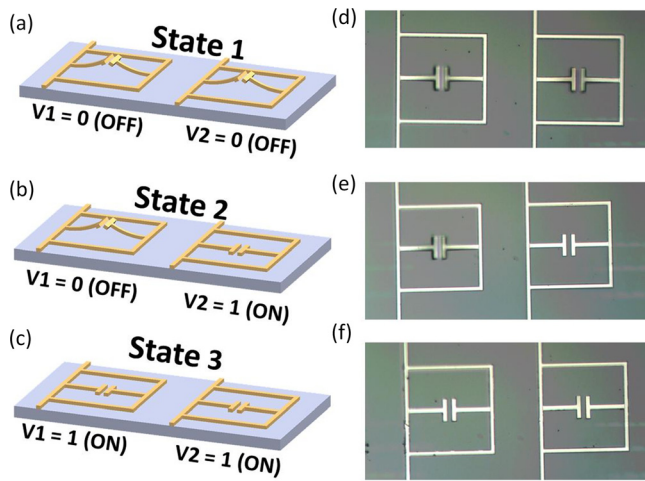


FIG. 3. (a)–(c) Illustration of the three configuration states of the unit cell that can be realized. (d)–(f) The corresponding optical microscope images.

either of the voltages to higher values while keeping the other one at 0 V. Finally, when high voltage is applied to both V_1 and V_2 , the released arms in both eSRRs come in physical contact with Si substrate and this configuration is defined as **State 3**. The 50 nm thin Al_2O_3 layer acts as an isolation layer in the ON state to prevent the flow of high current between the arms and the Si substrate. This is critical for the reliable operation of the metamaterial as these currents would cause Joule's heating and locally weld the electrodes together.¹⁵

In order to elucidate the THz transmission performance of the digitally coded MEMS metamaterial, finite-difference time-domain modeling was performed. The THz wave was incident normally with the polarization along the gap bearing side of the eSRR. Fig. 4 shows the simulated transmission of the digital metamaterial in all three states. In **State 1**, the resonance dip is observed at 0.41 THz as shown by the black curve in Fig. 4. When one of the eSRRs is switched to the ON state, the transmission spectrum shows two observable resonances at 0.29 THz and 0.43 THz as shown by the red-

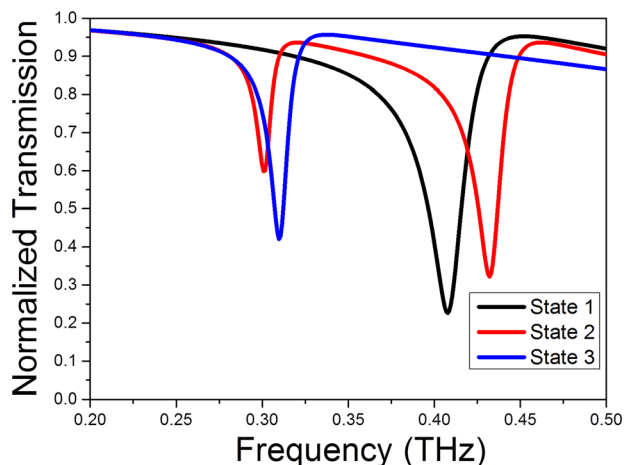


FIG. 4. Simulated THz transmission response of the digital metamaterial in three states: **State 1**, where all meta-bits are in OFF state (black curve); **State 2**, where half the meta-bits are in OFF state and other half in ON state (red curve); and **State 3**, where all meta-bits are in ON state (blue curve), respectively.

curve in Fig. 4. Finally, when both the eSRR meta-bits are switched to the ON state, the transmission spectrum has a resonance dip at 0.32 THz as shown by the blue-curve in Fig. 4. Surface current and scattered E_z field were studied to understand the resonance dynamics at various states of the metamaterial. As the polarization of the incident THz wave is along the split direction of eSRRs, two antiparallel currents are induced in the top and bottom rings of the eSRR at 0.41 THz and 0.32 THz as observed in Figs. 5(a) and 5(b). Due to the symmetry in the structure, only electrical resonance can be excited and is the electrical inductive-capacitive resonance (eLC). The eLC resonant frequency of the eSRR structure is $\omega = \sqrt{\frac{1}{LC}}$, where L and C refer to the effective inductance and capacitance in the metamaterial structure. When the central arms are released, the in-plane gap between them is also increased. Additionally, the out-of-plane gap between the released arms and Si substrate is also increased which is evident from the coupled E_z field between them as shown in Figs. 5(c) and 5(d). Hence, for eSRR in OFF state, both the in-plane and out-of-plane capacitances of the unit cell are decreased, thereby causing the effective capacitance of the eSRR to increase. The simulated OFF state resonant frequency of eSRR is at 0.41 THz, which is much higher than the ON state resonant frequency of 0.32 THz. The resonance mechanism of eSRR is however preserved at different reconfiguration states. More interestingly, for the metamaterial in **State 2**, half the eSRR meta-bits are in the OFF state, while the other half are in the ON state, and the transmission spectrum shows two distinctive resonances at 0.29 THz and 0.43 THz. Hence, by breaking the symmetry in the meta-bit configuration, the dual resonance behavior is realized. The number of resonators in both ON and OFF states is reduced by 50% and leads to lower resonance strength at the resonant frequencies, compared to **State 1** and **State 3** where 100% of eSRRs are in ON and OFF states, respectively. This concept can be further scaled up to multi-bit system, where more unit cells can be individually controlled, thereby leading to a more differentiable transmission value at a given frequency.

III. EXPERIMENTAL RESULTS

The experimental characterization of the binary coded digital metamaterial is done using THz time-domain spectroscopy (THz-TDS) system in a transmission mode. In all the measurements, the chamber is filled with nitrogen and the EM response is taken at room temperature. Similar to the simulation, the electric field of the input is aligned to be along the split gap and the propagation direction is normal to the metamaterial. In order to achieve active control, the metamaterial is hosted on a printed circuit board (PCB) with hole for THz transmission and the bond pads are connected to PCB through the wire bonding. The measured spectra of metamaterial are normalized with the Si substrate of the same thickness and are shown in Fig. 6. The measurement results match quite well with the simulation results. When the device is in **State 1**, the resonance frequency is around 0.37 THz. The resonance frequency shifts to 0.26 THz when

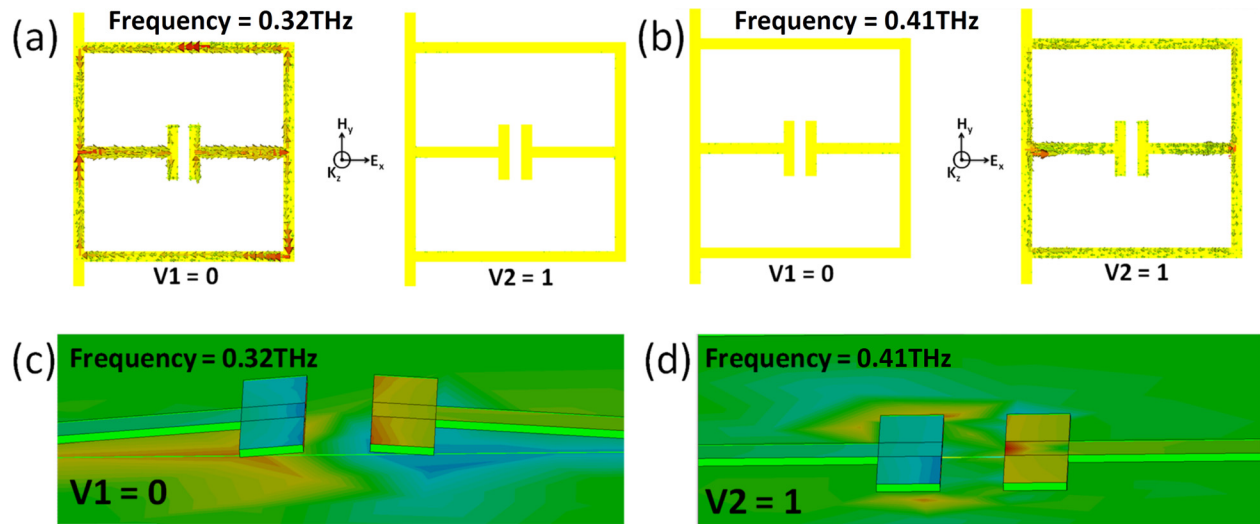


FIG. 5. Simulations of the surface current distribution of the unit cells at 0.41 THz and (b) 0.32 THz when the cantilevers are (a) suspended and (b) in contact with the substrate, respectively. Z-component of scattered electric field across the split gap at 0.41 THz and 0.32 THz when (c) the cantilevers are suspended and (d) the cantilevers are in contact with the substrate.

the configuration of the device is in **State 3**. Finally, when the device is in **State 2**, the resonance is split into 0.36 THz and 0.26 THz. The difference in the measured resonance frequencies in State 2 and the simulation is due to the limited duration set for the data acquisition in the time domain signal. In order to separate the two resonances from the eSRRs, the duration of the time domain data acquisition has to be extremely long. This is impractical and the extended duration of data acquisition also introduces the effects such as reflected signal from the Si substrate. This will interfere with the metamaterial resonances. The broadening of resonance in **State 1** could be caused due to the variation of release height in the central arms across the metamaterial. This broadening of resonance is also observed in **State 2** where half the eSRRs are in OFF state. This also causes the resonant frequencies to superimpose with each other and this further reduces the contrast in transmission. However, in **State 3** the resonance is much sharper as all the arms are in physical contact with Si substrate. By defining 0.26 THz as **F1** and 0.36 THz as **F2**, the high output intensity of more than

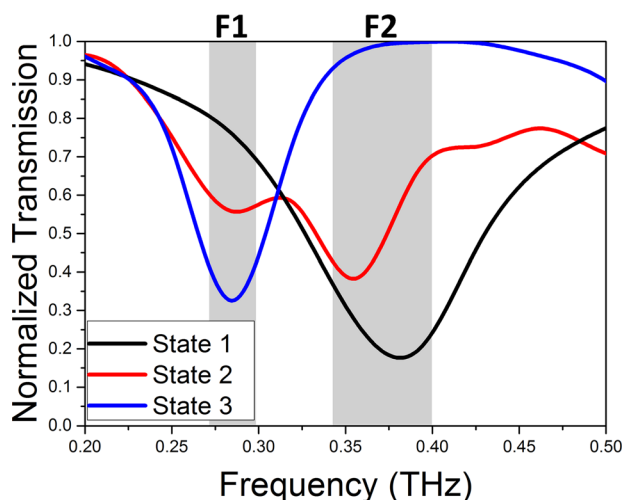


FIG. 6. Measured transmission spectra of the device in various states.

TABLE I. Output at F1 and F2 at various operating states.

V1	V2	Configuration	F1 (0.26 THz)	F2 (0.36 THz)
0	0	State 1	1	0
1	0	State 2	0	0
1	1	State 3	0	1
0	1	State 2	0	0
Analogous logic			NOR	AND

0.6 and the low output intensity of less than 0.6 are considered as logic “1” and “0,” respectively, and the results are summarized in Table I.

It is worth noting that for the cases of either **V1** or **V2** is “1,” they display the same measured output and hence can be classified as **State 2**. Based on the intensities of the outputs at **F1** and **F2** with the various configurations, the output at **F1** shows characteristics analogous to an **NOR** output, while the output at **F2** shows characteristics analogous to an **AND** output. The ideal threshold value for defining logic states would be the half of the transmission contrast of the metamaterial in **State 2** resonance frequencies. As a rule of thumb, it is better to separate the ON and OFF state resonance frequencies of the unit cell employed to avoid superposition of resonances in **State 2**. One of the possible ways would be to use the thinner thickness of the Al layer, which would provide much higher initial displacement and hence a higher frequency OFF state resonance, which is spectrally more isolated.²⁰

IV. CONCLUSION

In conclusion, the design, fabrication, and characterization of binary coded digital metamaterial are experimentally reported through the isolation of electrical controls to adjacent meta-bits for the terahertz spectral region. The digital metamaterial provides optical outputs that are analogous to that of logic outputs. Conventional eSRRs integrated with cantilever structures are used as the dynamically switchable

meta-bits. Different metamaterial unit cells can be readily adopted to further provide optical functionalities such as polarization control into the coded metamaterials. By varying the dynamic state of the meta-bits independently, three unique states of metamaterial are achieved, and the transmission outputs are analogous to **NOR** and **AND** at 0.26 THz and 0.36 THz, respectively. This work will enable the realization of multifunctional THz metamaterial and programmable metamaterial through further enhancement in control schemes, which will be one of the most disruptive technologies in the field of THz wave manipulation and applications.

ACKNOWLEDGMENTS

The authors acknowledge the financial support from the following research grants: Ministry of Education (MOE) Academic Research Fund (AcRF) (MOE2012-T2-2-154, WBS: R-263-000-A59-112); National Natural Science Foundation of China (61474078); and National Research Foundation (NRF) Competitive Research Programme (CRP) (NRF-CRP15-2015-02).

- ¹S. Koenig, D. Lopez-Diaz, J. Antes, F. Boes, R. Henneberger, A. Leuther, A. Tessmann, R. Schmogrow, D. Hillerkuss, R. Palmer, T. Zwick, C. Koos, W. Freude, O. Ambacher, J. Leuthold, and I. Kallfass, "Wireless sub-THz communication system with high data rate," *Nat. Photonics* **7**(12), 977–981 (2013).
- ²B. Sensale-Rodriguez, R. Yan, M. M. Kelly, T. Fang, K. Tahy, W. S. Hwang, D. Jena, L. Liu, and H. G. Xing, "Broadband graphene terahertz modulators enabled by intraband transitions," *Nat. Commun.* **3**, 780 (2012).
- ³D. Schurig, J. J. Mock, B. J. Justice, S. A. Cummer, J. B. Pendry, A. F. Starr, and D. R. Smith, "Metamaterial electromagnetic cloak at microwave frequencies," *Science* **314**(5801), 977–980 (2006).
- ⁴R. A. Shelby, D. R. Smith, and S. Schultz, "Experimental verification of a negative index of refraction," *Science* **292**(5514), 77–79 (2001).
- ⁵H. J. Lezec, J. A. Dionne, and H. A. Atwater, "Negative refraction at visible frequencies," *Science* **316**(5823), 430–432 (2007).
- ⁶J. Valentine, S. Zhang, T. Zentgraf, E. Ulin-Avila, D. A. Genov, G. Bartal, and X. Zhang, "Three-dimensional optical metamaterial with a negative refractive index," *Nature* **455**(7211), 376–379 (2008).
- ⁷O. Paul, C. Imhof, B. Lagel, S. Wolff, J. Heinrich, S. Hofling, A. Forchel, R. Zengerle, R. Beigang, and M. Rahm, "Polarization-independent active metamaterial for high-frequency terahertz modulation," *Opt. Express* **17**(2), 819–827 (2009).
- ⁸Y. C. Jun and I. Brener, "Electrically tunable infrared metamaterials based on depletion-type semiconductor devices," *J. Opt.* **14**(11), 114013 (2012).
- ⁹Z. Liu, C. Huang, H. Liu, X. Zhang, and C. Lee, "Resonance enhancement of terahertz metamaterials by liquid crystals/indium tin oxide interfaces," *Opt. Express* **21**(5), 6519–6525 (2013).
- ¹⁰R. Yan, B. Sensale-Rodriguez, L. Liu, D. Jena, and H. G. Xing, "A new class of electrically tunable metamaterial terahertz modulators," *Opt. Express* **20**(27), 28664–28671 (2012).
- ¹¹W. M. Zhu, A. Q. Liu, W. Zhang, J. F. Tao, T. Bourouina, J. H. Teng, X. H. Zhang, Q. Y. Wu, H. Tanoto, H. C. Guo, G. Q. Lo, and D. L. Kwong, "Polarization dependent state to polarization independent state change in THz metamaterials," *Appl. Phys. Lett.* **99**(22), 221102 (2011).
- ¹²W. M. Zhu, A. Q. Liu, T. Bourouina, D. P. Tsai, J. H. Teng, X. H. Zhang, G. Q. Lo, D. L. Kwong, and N. I. Zheludev, "Microelectromechanical maltese-cross metamaterial with tunable terahertz anisotropy," *Nat. Commun.* **3**, 1274 (2012).
- ¹³F. Ma, Y. Lin, X. Zhang, and C. Lee, "Tunable multiband terahertz metamaterials using a reconfigurable electric split-ring resonator array," *Light: Sci. Appl.* **3**(5), e171 (2014).
- ¹⁴F. Ma, Y. Qian, Y. S. Lin, H. Liu, X. Zhang, Z. Liu, M. L. Tsai, and C. Lee, "Polarization-sensitive microelectromechanical systems based tunable terahertz metamaterials using three dimensional electric split-ring resonator arrays," *Appl. Phys. Lett.* **102**(16), 161912 (2013).
- ¹⁵P. Pitchappa, C. P. Ho, L. Dhakar, Y. Qian, N. Singh, and C. Lee, "Periodic array of subwavelength MEMS cantilevers for dynamic manipulation of terahertz waves," *J. Microelectromech. Syst.* **24**(3), 525–527 (2015).
- ¹⁶C. P. Ho, P. Pitchappa, Y. Lin, C. Huang, P. Kropelnicki, and C. Lee, "Electrothermally actuated microelectromechanical systems based omega-terahertz metamaterial with polarization dependent characteristics," *Appl. Phys. Lett.* **104**(16), 161104 (2014).
- ¹⁷Z. Han, K. Kohno, H. Fujita, K. Hirakawa, and H. Toshiyoshi, "MEMS reconfigurable metamaterial for terahertz switchable filter and modulator," *Opt. Express* **22**(18), 21326–21339 (2014).
- ¹⁸Y.-S. Lin and C. Lee, "Tuning characteristics of mirrorlike T-shape terahertz metamaterial using out-of-plane actuated cantilevers," *Appl. Phys. Lett.* **104**(25), 251914 (2014).
- ¹⁹P. Pitchappa, C. P. Ho, L. Dhakar, and C. Lee, "Microelectromechanically reconfigurable interpixelated metamaterial for independent tuning of multiple resonances at terahertz spectral region," *Optica* **2**(6), 571–578 (2015).
- ²⁰P. Pitchappa, C. P. Ho, Y. Qian, L. Dhakar, N. Singh, and C. Lee, "Microelectromechanically tunable multiband metamaterial with preserved isotropy," *Sci. Rep.* **5**, 11678 (2015).
- ²¹T. J. Cui, M. Q. Qi, X. Wan, J. Zhao, and Q. Cheng, "Coding metamaterials, digital metamaterials and programmable metamaterials," *Light: Sci. Appl.* **3**(10), e218 (2014).
- ²²C. D. Giovampaola and N. Engheta, "Digital metamaterials," *Nat. Mater.* **13**(12), 1115–1121 (2014).
- ²³L. Liang, M. Q. Qi, J. Yang, X. Shen, J. Zhai, W. Xu, B. Jin, W. Liu, Y. Feng, C. Zhang, H. Lu, H. T. Chen, L. Kang, W. Xu, J. Chen, T. J. Cui, P. Wu, and S. Liu, "Anomalous terahertz reflection and scattering by flexible and conformal coding metamaterials," *Adv. Opt. Mater.* **3**(10), 1374–1380 (2015).
- ²⁴L. Gao, Q. Cheng, J. Yang, S. Ma, J. Zhao, S. Liu, H. Chen, Q. He, W. Jiang, H. Ma, Q. Wen, L. Liang, B. Jin, W. Liu, L. Zhou, J. Yao, P. Wu, and T. J. Cui, "Broadband diffusion of terahertz waves by multi-bit coding metasurfaces," *Light: Sci. Appl.* **4**(9), e324 (2015).
- ²⁵T. Driscoll, H. T. Kim, B. G. Chae, B. J. Kim, Y. W. Lee, N. M. Jokerst, S. Palit, D. R. Smith, M. Di Ventra, and D. N. Basov, "Memory metamaterials," *Science* **325**(5947), 1518–1521 (2009).
- ²⁶M. J. Dicken, K. Aydin, I. M. Pryce, L. A. Sweatlock, E. M. Boyd, S. Walavalkar, J. Ma, and H. A. Atwater, "Frequency tunable near-infrared metamaterials based on VO₂ phase transition," *Opt. Express* **17**(20), 18330–18339 (2009).
- ²⁷B. Gholipour, J. Zhang, K. F. MacDonald, D. W. Hewak, and N. I. Zheludev, "An all-optical, non-volatile, bidirectional, phase-change meta-switch," *Adv. Mater.* **25**(22), 3050–3054 (2013).
- ²⁸W. Y. Kim, H. D. Kim, T. T. Kim, H. S. Park, K. Lee, H. J. Choi, S. H. Lee, J. Son, N. Park, and B. Min, "Graphene-ferroelectric metadevices for nonvolatile memory and reconfigurable logic-gate operations," *Nat. Commun.* **7**, 10429 (2016).
- ²⁹D. A. Czaplewski, C. D. Nordquist, G. A. Patrizi, G. M. Kraus, and W. D. Cowan, "RF MEMS switches with—Contacts cycled to 10 billion cycles," *J. Microelectromech. Syst.* **22**(3), 655–661 (2013).
- ³⁰J. K. Gopal, A. T. Do, P. Singh, G. L. Chua, and T. T. H. Kim, "A cantilever-based NEM nonvolatile memory utilizing electrostatic actuation and vibrational deactuation for high-temperature operation," *IEEE Trans. Electron Devices* **61**(6), 2177–2185 (2014).
- ³¹D. R. Chowdhury, R. Singh, M. Reiten, J. Zhou, A. J. Taylor, and J. F. O'Hara, "Tailored resonator coupling for modifying the terahertz metamaterial response," *Opt. Express* **19**(11), 10679–10685 (2011).
- ³²D. R. Chowdhury, N. Xu, W. Zhang, and R. Singh, "Resonance tuning due to Coulomb interaction in strong near-field coupled metamaterials," *J. Appl. Phys.* **118**(2), 023104 (2015).
- ³³P. Pitchappa, M. Manjappa, C. P. Ho, Y. Qian, R. Singh, N. Singh, and C. Lee, "Active control of near-field coupling in conductively coupled microelectromechanical system metamaterial devices," *Appl. Phys. Lett.* **108**(11), 111102 (2016).
- ³⁴P. Pitchappa, M. Manjappa, C. P. Ho, R. Singh, N. Singh, and C. Lee, "Active control of electromagnetically induced transparency analogue in terahertz MEMS metamaterial," *Adv. Opt. Mater.* (published online).